



ENVIRONMENTAL HEALTH PERSPECTIVES

<http://www.ehponline.org>

Size-Dependent Deposition, Translocation, and Microglial Activation of Inhaled Silver Nanoparticles in the Rodent Nose and Brain

Esther Shin Patchin, Donald S. Anderson, Rona M. Silva,
Dale L. Uyeminami, Grace M. Scott, Ting Guo,
Laura S. Van Winkle, and Kent E. Pinkerton

<http://dx.doi.org/10.1289/EHP234>

Received: 3 June 2015

Revised: 15 October 2015

Accepted: 26 April 2016

Published: 6 May 2016

Note to readers with disabilities: *EHP* will provide a [508-conformant](#) version of this article upon final publication. If you require a 508-conformant version before then, please contact ehp508@niehs.nih.gov. Our staff will work with you to assess and meet your accessibility needs within 3 working days.



Size-Dependent Deposition, Translocation, and Microglial Activation of Inhaled Silver Nanoparticles in the Rodent Nose and Brain

Esther Shin Patchin¹, Donald S. Anderson¹, Rona M. Silva¹, Dale L. Uyeminami¹, Grace M. Scott¹, Ting Guo², Laura S. Van Winkle^{1,3}, and Kent E. Pinkerton^{1,3,4}

¹Center for Health and the Environment, University of California, Davis, California, USA;

²Department of Chemistry, University of California, Davis, California, USA; ³Department of Anatomy, Physiology and Cell Biology, School of Veterinary Medicine, University of

California, Davis, California, USA; ⁴Department of Pediatrics, School of Medicine, University of California, Sacramento, California, USA

Address correspondence to Kent E. Pinkerton, Center for Health and the Environment, University of California, One Shields Avenue, Davis, California 95616 USA. Telephone: 530-752-8334. E-mail: kepinkerton@ucdavis.edu

Short running title: Size Dependent Activity of AgNP in Nose and Brain

Acknowledgments: The authors thank Janice Peake, Imelda Espiritu, and Alexa Pham for technical assistance during the course of this study, Joel Commisso for silver analysis (UC Davis Interdisciplinary Center for Inductively Coupled Plasma Mass Spectrometry) and Dr. Neil Willits for statistical analysis and guidance (UC Davis Statistical Laboratory). Grant support for this study was from U01 ES020127. The silver nanomaterials used in this study were procured, characterized and provided to investigators by NIEHS Centers for Nanotechnology Health

Implications Research (NCNHIR) Consortium. We also acknowledge support from grants T32 HL086350 (ESP), P42 ES004699 (DSA), NIOSH Grant 0H07550 (RMS) and P30 ES023513.

Competing financial interests: The authors declare they have no competing financial interests

ABSTRACT

Background: Silver nanoparticles (AgNP) are present in personal, commercial, and industrial products, which are often aerosolized. Current understanding of the deposition, translocation, and health-related impacts of AgNP inhalation is limited.

Objectives: To determine 1) the deposition and retention of inhaled Ag in the nasal cavity from nose-only exposure; 2) the timing for Ag translocation to and retention/clearance in the olfactory bulb (OB); and 3) whether the presence of Ag in the OB affects microglial activity.

Methods: Male Sprague-Dawley rats were exposed nose-only to citrate-buffered 20 or 110 nm AgNP (C20 or C110, respectively) or citrate buffer alone for six hours. The nasal cavity and OB were examined for the presence of Ag and biological responses up to 56 days post exposure (8 weeks).

Results: The highest nasal Ag deposition was observed at Day 0 for both AgNP sizes. Aerosolized C20 resulted in rapid translocation of Ag to the OB and microglial activation at Days 0, 1 and 7. In contrast, inhalation of C110 resulted in a gradual but progressive transport of Ag to and retention in the OB, with a trend for microglial activation to variably be above control.

Conclusions: This study demonstrates that after a six-hour inhalation exposure in rats to 20 and 110 nm AgNP at a single point in time, Ag deposition in the nose, the rate of translocation to the brain, and subsequent microglial activation in the OB, differed depending on AgNP size and time since exposure.

INTRODUCTION

Silver nanoparticles (AgNP) are widely used for their anti-microbial activity and are found in textiles, cosmetics, food, and medical supplies. AgNP are currently being considered for use as anti-cancer agents (Wei et al. 2015). Approximately 50% of all nanoparticles in commercial use today are composed of silver (The Project on Emerging Nanotechnologies 2015). Exposure to AgNP can occur through dermal absorption, oral ingestion, or inhalation. Inhalation of AgNP may occur during manufacturing, cloud seeding, or spraying for wound treatment as well as through the use of AgNP as an aerosol disinfectant (Genter et al. 2012) or over-the-counter homeopathic spray for treatment of respiratory infections (Silver Lungs 2009; The Silver Edge 2012). Due to their small size, AgNP can easily penetrate into the deep lung, which possesses an immense surface area for deposition, and potentially transport to the systemic circulation. AgNP can also enter the nasal cavity and translocate to the brain via the olfactory epithelium, a direct connection between the nose and brain (Kovacs 2004).

Previous studies have shown nanoparticles, viruses, and molecules can bypass the blood-brain barrier and be transported from the olfactory epithelium in the nasal cavity to the olfactory bulb (OB) in the forebrain (Illum 2000; Mistry et al. 2009b). Three possible pathways have been suggested: 1) transcellular transport across sustentacular cells of the olfactory epithelium, 2) paracellular transport through junctions of the olfactory epithelium, or 3) intracellular transport through axonal movement via olfactory nerve fascicles to the synaptic junctions within the OB (Illum 2000; Shepherd 1994). Nanoparticle translocation along axons of olfactory nerve fascicles and accumulation in the OB have been previously studied (Aschner 2009; De Lorenzo 1960; Elder et al. 2006; Elder et al. 2009; Hopkins et al. 2014; Oberdorster et al. 2004, Patel et al. 2011).

AgNP toxicity has been associated with the formation of Ag cations (Ag^+), biochemically active agents (Brett 2006) that cause cytotoxic (Chernousova and Epple 2013; Loza et al. 2014; Xiu et al. 2012) and inflammatory responses (Wang et al. 2014) independent of the parent AgNP. The toxicity of Ag^+ may be due to its interaction in biochemical processes with proteins, nucleic acids, and cell membranes (Chernousova and Epple 2013). Smaller (20 nm) AgNP were found to have faster dissolution rates and Ag^+ formation than larger (110 nm) AgNP (Davidson et al. 2014; Wang et al. 2014).

While human health effects from AgNP exposure have been reported following dermal or oral administration (Gavanji et al. 2013), to the best of our knowledge, there are currently no published peer-reviewed studies that discuss the effects of AgNP inhalation in humans. Inhalation studies with animals demonstrated deposition of Ag in the lung and translocation to other organs (Anderson et al. 2015; Braakhuis et al. 2014; Genter et al. 2012; Ji et al. 2007; Sung et al. 2009). Toxic responses included epithelial erosion, proteinaceous exudates, and/or presence of inflammatory cells in the nasal cavity (Genter et al. 2012), airways and alveoli (Braakhuis et al. 2014; Sung et al. 2009) as well as consequent bile duct hyperplasia in the liver (Sung et al. 2009). The magnitude of these changes appear to be dependent on the dose and/or size of the AgNP used (Braakhuis et al. 2014; Sung et al. 2009).

The objectives of this study were to determine 1) the deposition and retention of Ag in the nasal cavity following inhalation exposure; 2) the timing for Ag translocation and retention/clearance in the OB; and 3) whether the presence of Ag in the OB affects activity of microglial cells, the resident macrophages of the OB and brain. Nasal cavities and OBs in this study were obtained from the same animals used in the Anderson et al. (2015) study, where a single acute inhalation dose of 20 or 110 nm AgNP (C20 or C110, respectively) was delivered

over a period of 6 hours, and biological samples were obtained immediately after exposure (T0) as well as 1 (T1), 7 (T7), 21 (T21), and 56 (T56) days post exposure.

METHODS

Particles

AgNP [20 or 110 nm in diameter (nanoComposix, Inc., San Diego, CA)] were suspended in citrate buffer (Fisher Scientific, Pittsburg, PA). The AgNP were procured, characterized, and supplied by the NIEHS Centers for Nanotechnology Health Implications Research (NCNHIR) Consortium (NIH 2015). Citrate stabilized the particles by creating electrostatic repulsion, thus preventing AgNP aggregation and enabling control of the final particle size (Tolaymat et al. 2010). Physicochemical characterization of the AgNP is described previously by Anderson et al. (2015), Silva et al. (2014), and Wang et al. (2014).

Animals

Ten- to twelve-week old male Sprague Dawley rats (Harlan Laboratories, Livermore, CA) were used to maintain consistency with other studies (Anderson et al. 2015; Ji et al. 2007; Silva et al. 2014; Sung et al. 2009). Upon arrival, rats were randomly assigned to three groups: 1) C20-, 2) C110-, or 3) citrate control-treated (n=8 per AgNP treatment group per time point, and n=8 for citrate control). The rats were allowed to acclimate for one week prior to exposure, housed two per cage, and given access *ad libitum* to water and a standard laboratory rodent diet (Purina Mills, St Louis, MO) except during exposure periods. Animals were handled under

protocols in accordance with the Guide for the Care and Use of Laboratory Animals, and the Institutional Animal Care and Use Committee of the University of California, Davis.

Aerosolization of AgNP

Rats were acclimated in inhalation exposure tubes (Teague Enterprises, Woodland, CA, USA) for 1 week prior to the scheduled exposure to simulate exposure conditions. Animals were trained to enter and remain in the exposure tubes until released. Time in the tube increased up to six hours at a gradual rate over the training week. This served to minimize/prevent confinement stress during the actual AgNP aerosol exposure period.

Rats were exposed via nose-only inhalation to C20, C110, or citrate buffer for six hours. The aerosolization regimen has been previously described (Anderson et al. 2015). Briefly, a 6-jet collision nebulizer (Mesa Labs, Waltham, MA) was used to aerosolize the AgNP suspensions into fine droplets. Water was removed from the droplets using two TSI diffusion dryers (TSI, Shoreview, MN), and particle charge was neutralized with a Krypton-85 source. Samples were collected throughout the exposure period for aerosol characterization as previously described by Anderson et al. (2015) for gravimetric, x-ray fluorescence (XRF), cascade impactor, transmission electron microscope (TEM), and real-time size mobility particle scanner (SMPS) measurements. Airborne particle number was also calculated based on the airborne concentration of Ag collected by XRF analysis. Estimated Ag deposition in the nose normalized to surface area of the rat nasal epithelium was $4 \mu\text{g}/\text{cm}^2$ or $1 \mu\text{g}/\text{cm}^2$ after exposure to aerosolized suspensions of C20 or C110, respectively. This dose was selected to approximate human exposure after one day of light work in a worst-case occupational scenario, based on assumptions and calculations

described in detail in Supplemental Material, “Relating experimental rodent inhalation of AgNP to human occupational exposure”.

Necropsy and tissue collection

Biological samples were collected at all post-exposure time points. All rats were anaesthetized by intraperitoneal injection of sodium pentobarbital (120 mg/kg) and euthanized via exsanguination. The nasal epithelium and OB from five animals per group were collected and frozen in liquid nitrogen for silver detection via inductively-coupled plasma mass spectroscopy (ICP-MS). In addition, the OBs from three rats per group were fixed in 4% paraformaldehyde for silver detection via autometallography, and OBs from these same animals were also fixed in 4% paraformaldehyde for microglial examination and cytokine expression assays.

Preparation of tissue sections

To detect silver by ICP-MS, the entire head was cut sagittally to expose the nasal epithelium. All the strippable epithelium including the septal and turbinate walls, was collected in order to maintain the collection consistency between rats.

The nasal epithelium and whole OBs were placed into liquid nitrogen in 15 mL conical tubes. Frozen tissues were lyophilized using LabconcoFreeZone 2.5 (Kansas City, MO) for 48 hours after which tissue weights were determined. The tissues were subsequently digested using equal parts of 70% trace metal grade nitric acid (Fisher Scientific) and 30% hydrogen peroxide (EMD Millipore, Billerica, MA). Digestion in nitric acid occurred at 70°C for two hours, cooled to room temperature (25°C) for one hour. Subsequent digestion in an equal volume of hydrogen peroxide occurred at 70°C for fifteen hours followed by cooling to room temperature. All samples were brought to a known volume and diluted 5:1 with milli-Q water.

Samples were analyzed at the UC Davis Interdisciplinary Center for Plasma Mass Spectrometry using an Agilent 7500CE ICP-MS (Agilent Technologies, Palo Alto, CA). Silver concentration ($\mu\text{g Ag/g tissue}$) was calculated from the known tissue weight (g), sample volume (mL), and measured Ag content (ng/mL). The mean and standard error of silver concentration were calculated, and statistical differences were compared between C20- or C110-treated and citrate control groups at each time point. The hypothetical number of AgNP in the nose and OB was also estimated from the mass of Ag detected by ICP-MS and normalized to known tissue weight. For these calculations, we assumed that the AgNP maintained a spherical shape with no dissolution throughout the post-exposure period.

For silver detection via autometallography, nasal sections were deparaffinized with toluene, hydrated in decreasing concentrations of alcohol, and stained with equal volumes of silver enhancement kit for light and electron microscopy (Ted Pella Inc., Redding, CA) for 15 minutes. Sections were then dehydrated in increasing concentrations of alcohol and toluene and coverslipped with Clear Mount permanent mounting medium (Thermo Fisher Scientific, Waltham, MA). All images were observed using a Zeiss Axio Lab.A1 microscope and detection of stains were observed.

Microglial activation and TNF- α detection in the olfactory bulb

For microglial examination and cytokine expression, OBs were fixed in 4% paraformaldehyde for seven days and embedded in a sagittal orientation in paraffin. Sections 5 μm thick were cut, deparaffinized with toluene, hydrated in decreasing concentrations of alcohol, and rinsed with phosphate buffered saline with Tween (PBST; Sigma Aldrich, St. Louis, MO) before antigen retrieval. Slides were immersed in citric acid (Thermo Fisher Scientific; pH = 6)

for 30 seconds at 125°C for antigen retrieval, followed by 10 seconds at 85°C. Sections were then cooled for 15 minutes, rinsed with PBST for 3 minutes and with 3% hydrogen peroxide for 5 minutes, washed in PBST 3 times at 3 minutes each and followed by a non-specific block, Protein Block (Dako, Carpinteria, CA) for 30 minutes at room temperature. The sections were then incubated with the primary antibody, anti-Iba1 (ionized calcium-binding adapter molecule 1) antibody (Abcam Inc., Cambridge, MA) to visualize microglial cells in a state of rest or activation for 3 hours or anti-TNF- α (tumor necrosis factor alpha) antibody (Abcam Inc.) for 1 hour at room temperature. Sections were washed with PBST 3 times for 3 minutes each, then incubated in secondary antibody, biotinylated affinity-purified goat anti-rabbit IgG (Vector Laboratories, Burlingame, CA) for 1 hour at room temperature or HRP-labeled polymer (rabbit) (Dako, Carpinteria, CA) for 30 minutes at room temperature. The sections were again washed with PBST for 5 minutes, incubated with Avidin/Biotin Complex (Vector Laboratories) for 30 minutes at room temperature, and rinsed with PBST again 3 times at 5 minutes each. The sections were then incubated with DAB and substrate (Dako, Carpinteria, CA) for 5 minutes, counterstained with Harris' Hematoxylin (MasterTech, Inc., Lodi, CA), and coverslipped with Clear Mount permanent mounting medium (Thermo Fisher Scientific).

Microglial morphology was observed to determine whether they were resting or activated. Briefly, resting microglia were defined as cells with at least two highly branched (ramified) processes extending at least twice the length of a highly elliptical nucleus. Activated microglia were defined as cells with significantly shortened branching processes extending from a slightly enlarged cell nucleus (Figure 1). Microglia were counted in ten randomly-sampled, non-overlapping fields per histological section per animal and observed at an objective magnification of 20x using a Zeiss Axio Lab A1 microscope. Resting and activated microglia

were also counted in identical histological fields for each animal to a total of 50 cells/animal, and the ratio of active to total cells was calculated. The mean value and percent difference (compared to control) were determined for each exposure group at each time point. The incidence of TNF- α staining was measured in the OB using ImageJ (Rasband 2007-2014) with a 5X objective on the same Zeiss microscope. The intensity of TNF- α staining within total areas of expression was determined for each exposure group at each time point. Three animals per AgNP treatment group per time point were examined along with six control animals.

Silver transport analysis

The percentage of Ag translocation at T0 for C20 and at T56 for C110 was calculated to determine how much Ag in the nose transported to the OB via the olfactory region of the nasal cavity. Based upon the computational fluid dynamics model proposed by Garcia and Kimbell (2009), about 24.55% and 35% of C20 and C110 in the nose, respectively, deposited in the olfactory region. These percentages were then used with our data of total Ag deposition in the nasal cavity at T0 for C20 and at T56 for C110 to determine how much of the total Ag deposition was deposited only in the olfactory region. The percentage of Ag translocation was then calculated by the total Ag in the OB and Ag deposited in the olfactory region.

Statistical analysis

All the data presented here were analyzed using JMP 10.0.0 statistical software (Cary, NC). No outliers were identified, with outliers being quantified as how far the value was from the others using Grubbs' test. The ICP-MS data were first tested for deviations from the normality and homoscedasticity (equal variance) assumptions of Analysis of Variance (ANOVA) using Shapiro-Wilk (on model residuals) and Levene tests, respectively. To achieve normal

distributions, data were log-transformed (\log_{10}). ANOVA and Post hoc Tukey HSD tests were performed for all the ICP-MS and particle number data to determine specific significant differences between treatment groups. These tests were performed using a significance level of $p < 0.05$. Significance for microglial activation was determined by ANOVA and least significant difference (LSD) student t-test to determine significant differences ($p < 0.05$) at each time point due to exposure type (C20 or C110 versus control).

RESULTS

Particle characterization and aerosolization

AgNP characteristics were determined by Anderson et al. (2015) and are summarized in Table 1. Anderson et al. (2015) observed minimal changes in the hydrodynamic diameter of AgNP determined by dynamic light scattering (DLS) in suspension before (from sealed containers) and after exposure (from the nebulizer). Particle mass concentration from the generated aerosols was determined gravimetrically. In addition, airborne particle number concentrations were estimated using the XRF-determined silver mass concentrations (Anderson et al. 2015) (Table 1).

Silver content in the nasal epithelium and OB

The limit of detection (LOD) was 11 ppb, with all data reported as measured values without regard to the LOD. Silver concentrations in the nasal epithelium were significantly higher than in controls at all time points post exposure to both C20 and C110 (Figure 2A). For both particles, concentrations were highest immediately after treatment (T0) and lowest at T56,

with significantly lower concentrations relative to T0 for C20 at T1, T21, and T56 and for C110, at T21 and T56. Although some data points are below the detection limit (citrate buffer, C20 at T1-T56, and C110 at T0-T1), if viewed as measured, the trends show that after exposure to C20 (versus control), approximately 4% (0.013 $\mu\text{g/g}$ in the OB at T0 after C20 exposure vs. 0.34 $\mu\text{g/g}$ in the nasal epithelium at T0 after C20 exposure) of the Ag was translocated from the nose to the OB, and the concentration of silver detected in the OB at T0 (0.013 \pm 0.0042) was significantly higher than the concentration in controls (Figure 2B). At subsequent time-points after C20 exposure, the concentration of silver in the OB of treated animals was not significantly different from background levels in controls. However, after exposure to C110, the concentration of silver in the OB at T21 and T56 was significantly higher than the T0 concentration in C110 exposed animals at all four subsequent time points (Figure 2B). Silver detection via autometallography showed very sparse amounts only in C20 exposed animals at T0. Other levels and time points failed to clearly show Ag ions or particles.

Microglial activation and cytokine expression

Microglial morphology in the OB was observed and differentiated between resting and activated states in order to determine whether the two AgNP types elicited responses (Figure 1). Compared to controls, proportions of activated microglia in the OB were significantly higher among C20 treated animals at T0, T1, and T7, and in C110 treated animals at T0 (see Supplemental Material Table S1 for values in individual animals and Figure 3 for mean values). The mean proportion of activated microglia after C20 exposure decreased after T1 such that proportions were not significantly different from control animals at T21 and T56 and were

significantly higher at T0 and T1 than at T56, when the mean proportion of activated microglia was only 3% higher ($\pm 12\%$) than the mean in controls. Conversely, C110 produced a variable pattern, with minimal activation at T1 and T7 ($11\% \pm 11\%$ and $10\% \pm 2\%$, respectively), in contrast to a relatively high degree of microglial activation at T0, T21 and T56 ($37\% \pm 5\%$, $34\% \pm 5\%$, and $31\% \pm 1\%$, respectively) with significance shown only at T0 (Figure 3). Mean microglial number/field was significantly lower than in controls for C20 animals at T0, suggesting a transient cytotoxic response to nanoparticles in the OB (Figure 4). Although the mean microglial number/field at T0 was lower than in C110 animals than controls, the difference was not significant, and there were no significant differences from controls at any other remaining time point for either AgNP exposure group.

TNF- α staining, although observed in the OB, was not found to be significantly different from that of the controls at any time point for either treatment group (data not shown).

Silver transport to the olfactory bulb via the olfactory region

The amount of Ag deposited in the olfactory region of the nose was $0.08 \mu\text{g Ag/g}$ tissue and $0.15 \mu\text{g Ag/g}$ tissue for C20 and C110, respectively. The percentage of silver translocated to the OB from the olfactory region of the nose was 16% and 9% at T0 for C20 and at T56 for C110, respectively.

DISCUSSION

Short-term inhalation of AgNP resulted in the accumulation of silver in the OB over time, with some differences according to nanoparticle size. Following a single six hour inhalation

exposure, C20 and C110 AgNP were deposited and taken up in the epithelium of the nose, where they were retained and subsequently transported to the OB. Silver content in the nose and OB was monitored up to 56 days (8 weeks) post exposure and correlated to varying degrees to microglial responses in the OB. These findings suggest 1) AgNP size does not affect retention/clearance of Ag in the nose or OB; 2) C20 AgNP readily translocate to the OB where they elicit an immediate response; and 3) C110 AgNP accumulate and elicit a varied response in the OB immediately after exposure and at later time points.

Irrespective of the original particle size, Ag concentrations in the nose remained significantly higher than in controls up to 8 weeks post-inhalation. We believe that this persistence is most likely due to interstitial and/or intraepithelial localization, as was previously noted in the lungs of the same animals (Anderson et al. 2015). However, autometallography in this study failed to conclusively demonstrate the precise localization of Ag in the nose perhaps due to relatively small amounts of Ag remaining there compared with the lung. Ag in the nasal cavity can be cleared from the respiratory tract via several pathways: 1) mucocilliary movement to the nasopharynx and into the gastrointestinal tract; 2) translocation to the circulatory system; 3) translocation to the lymphatic system; and 4) translocation to the OB. We observed significant Ag in the OB at T0 for C20 and at T21 and T56 for C110 compared to the control, which suggests that Ag is transported from the nose to the OB.

Previous studies report transport of nanoparticles to the OB via the olfactory system in the nose (Elder et al. 2009; Hopkins et al. 2014; Oberdorster et al. 2004) and higher levels of Ag in the OB compared to the rest of the brain as measured by atomic absorption spectroscopy (Ji et al. 2007; Sung et al. 2009). Genter et al. (2012) visualized Ag in the OB and cells lining the lateral ventricle via autometallography following intranasal administration and surmised that

high Ag deposition in the OB, which is located close to the inhalation site compared to the rest of the brain, suggests that Ag particles reach the brain via the nose. The investigators showed aggregation of Ag in the turbinated areas of the nasal cavity lined with olfactory epithelium, which is one of the main direct portals of entry to the OB (Genter et al. 2012).

Garcia and Kimbell (2009) reported that even though total nasal deposition (of inhaled 1-100 nm particles) decreases with increasing particle size, a higher proportion of larger nanoparticles deposit in the olfactory region compared to other regions (i.e., respiratory, squamous, and transitional epithelium) of the nasal cavity. Using the computational fluid dynamics model proposed by Garcia and Kimbell (2009), we estimated that olfactory deposition of C20 and C110 would be approximately 25% and 35% of the total nasal deposition, respectively. Based on this information and known Ag concentration determined by ICP-MS, approximately 16% of C20 is translocated by T0 and 9% of C110 translocated by T56 from the olfactory region of the nose to the OB of the brain (see Supplemental Material, Table S2). These estimates are similar to those reported by Oberdorster et al. (2004), who showed consistent accumulation of 36 nm ¹³C (carbon particles) and approximately 20% translocation from the olfactory region to the OB. In the Oberdorster study, axonal transport via the olfactory sensory neurons was the main translocation pathway over the seven day post-exposure period.

We believe that the physicochemical properties (size and dissolution rate) of C20 and C110 most likely are responsible for their different deposition in the OB over time. While C20 AgNP are small enough to be rapidly transported through the olfactory axons, C110 AgNP are not. Mistry et al. (2009a) showed that 100 nm polystyrene nanoparticles were unable to translocate from the olfactory axon, which tapers off through the basement membrane, to the OB in mice. Based on a previous publication reporting that rabbit olfactory axons have an average

diameter of approximately 200 nm and many axons less than 100 nm (De Lorenzo 1960; Mistry et al. 2009b), we surmise that the average diameter of rat olfactory sensory neurons is likely less than or equal to 100 nm. Although it is unknown whether Ag present in the OB is ionic or particulate, we speculate that Ag from C110 did not travel from the nose to the OB by olfactory sensory neuron transport because solid 110 nm particles are unlikely to “fit” in the axons. However, if the diameter of rat olfactory axons is larger than 100 nm, it may be possible for C110 AgNP to transport (slow anterograde) from the nose to the OB. In this case, transport favors dissolved Ag ions or smaller AgNP formed after the initial dissolution event.

Differences in OB Ag content at various time-points post exposure to C20 (versus C110) may be due to the ability of C20 to directly transport along the axons and dissolve relatively fast. Rapid ion dissolution is enabled by the presence of organic molecules (Loza et al. 2014) and oxidation (Liu et al. 2012). Mucin in the nose consists of carbohydrates and heavily glycosylated proteins rich in serine and threonine residue (Thornton et al. 2008), which can aid in particle dissolution, and the nose is a continuous site of oxidation. Particle size can also contribute to dissolution, with smaller citrate-coated C20 undergoing more rapid dissolution than larger C110 (Wang et al. 2014; Zhang et al. 2011). While C20 may immediately dissolve to form Ag^+ and (in subsequent ionic reactions) form smaller AgNP, C110 continuously sheds, as evidenced by concurrent high concentrations of Ag^+ around the parent AgNP over time (Davidson et al. 2014). C20 could be rapidly transported to the OB with highest deposition at the earliest time point (T0). On the other hand, due to a slower dissolution process, C110 may not reach the OB in all animals until approximately 21 days because C110 produce more Ag^+ ions that continuously go through cycles of small particle formation and dissolution until the parent AgNP are depleted

(Davidson et al. 2014). Thus, the time for transport and accumulation of C110 Ag in the OB is extended.

Previous studies confirm the presence of Ag in the OB with no observable histopathology (Ji et al. 2007; Sung et al 2009; Genter et al 2012). Only Genter et al. examined microglial activation due to Ag exposure: three groups of mice were exposed to sterile water or different doses of 25 nm AgNP and sacrificed at 1 or 7 day(s) after a single intranasal instillation. Despite detection of Ag in the OB, no inflammatory cell infiltrates or microglial activation was observed. The Genter et al. (2012) study and our study differ by AgNP coating. Whereas we coated the AgNP with citrate to prevent aggregation, Genter et al. (2012) did not and observed (by DLS) agglomeration of the 25 nm AgNP into 118 nm aggregates. This aggregation could have hindered the release of Ag⁺ for more than 7 days, thereby preventing the observation of microglial activation. Indeed, the current study suggests that larger (C110) AgNP do not produce a significant amount of Ag⁺ immediately following deposition based on a significant amount of silver in the OB only found 21 days postexposure.

In this study, microglial activation was observed as an initial response. Although microglial activation can be beneficial to cellular maintenance and clearance of foreign substances, if prolonged and over-stimulated, this process can be detrimental due to the release of toxic factors, such as free radicals, and potentiation of neuronal loss and damage (Block et al. 2007). After exposure to C20, animals had a significantly lower mean total microglial number compared with controls (T0; Figure 4), while the proportion of activated microglial cells was significantly higher than in controls at T0 and T1, but comparable to controls by T56 (Figure 3). Exposure to C110 produced the highest microglial activation at T0 that then declined by T7 and increased again (non-significantly) at T21 and T56. However, no significant differences in TNF-

α staining were noted between treatment and control groups at any time point, suggesting the lack of a robust pro-inflammatory cytokine response during microglial activation in this study.

The microglial activation seen here may be caused by Ag^+ . A correlation has been noted between toxicity and dissolution of Ag^+ from AgNP in vitro (Brett 2006; Chernousova et al. 2013; Wang et al. 2014). The faster dissolution rate of C20 could explain the higher activation of microglia at earlier (versus later) time points (T0 and T1). Discrepancies between the amount of Ag deposition and microglial activation post exposure to C110 may be explained by a slower Ag^+ production rate. While the presence of Ag at T0 may have been too low to detect in the OB, trace amounts of Ag^+ could cause microglial activation. By T1, Ag^+ could also reduce and reform into small AgNP, making Ag^+ unavailable to elicit a response. Because AgNP are continuously shedding Ag^+ until their depletion, T56 could be the time when these Ag^+ ions are most present, thus causing higher microglial activation at this time point. A previous study by Soderstjerna et al. (2014) showed microglial activation in cultured neural retina explants from exposure to 20 or 80 nm AgNP at final concentrations of 0.0035 and 0.22 $\mu\text{g}/\text{mL}$, respectively. Although only 80 nm AgNP produced significant numbers of activated microglia in contrast to control, 20 nm AgNP produced a non-significant elevation. To the best of our knowledge, there are no other reports demonstrating microglial activation by AgNP.

CONCLUSION

This study is the first to demonstrate the ability of Ag to be deposited, translocated and retained from the nose to the brain (OB) at levels sufficient to cause microglial activation for two different-sized AgNP up to 56 days post exposure following a single six hour inhalation period. The long-term retention of measurable silver in the nasal cavity and the OB is also an important

finding. The mechanism of microglial activation, the physicochemical state of Ag in tissues over time, and the potential to elicit neurological effects following inhalation of differently sized AgNP clearly merits further investigation. The study provides useful information to increase awareness of the possible importance in regulation of inhaled AgNP in occupational settings and demonstrates the potential risk associated with using aerosolized AgNP as holistic therapeutic or anti-microbial agents.

REFERENCES

- Anderson DS, Patchin ES, Silva RM, Uyeminami DL, Sharmah A, Guo T, et al. 2015. Influence of particle size on persistence and clearance of aerosolized silver nanoparticles in the rat lung. *Toxicol Sci* 144(2):366-381.
- Aschner M. 2009. Nanoparticles: transport across the olfactory epithelium and application to the assessment of brain function in health and disease. *Prog Brain Res* 180:141-152.
- Block ML, Zecca L, Hong JS. 2007. Microglia-mediated neurotoxicity: uncovering the molecular -mechanisms. *Nat Rev Neurosci* 8:57-69.
- Braakhuis HM, Gosens I, Krystek P, Boere JAF, Cassee FR, Fokkens PHB, et al. 2014. Particle size dependent deposition and pulmonary inflammation after short-term inhalation of silver nanoparticles. *Part Fibre Toxicol* 11:49.
- Brett DW. 2006. A discussion of silver as an antimicrobial agent: alleviating the confusion. *Ostomy Wound Manage* 52(1):34-41.
- Chernousova S, Epple Matthias. 2013. Silver as antibacterial agent: Ion, nanoparticle, and metal *Angew Chem Int Ed* 52-1636-1653.
- Davidson RA, Anderson DS, Van Winkle LS, Pinkerton KE, Guo T. 2014. Evolution of silver nanoparticles in the rat lung investigated by x-ray absorption spectroscopy. *J Phys Chem* 119(2):281-289.
- De Lorenzo AJD. 1960. Electron microscopy of the olfactory and gustatory pathways. *Ann Otol Rhino Laryngol* 69:410-420.

Elder A, Gelein R, Silva V, Feikert T, Opanashuk L, Carter J, et al. 2006. Translocation of inhaled ultrafine manganese oxide particles to the central nervous system. *Environ Health Perspect* 114:1172-1178.

Elder A, Lynch I, Grieger K, Chan-Remillard S, Gatti A, Gnewuch H, et al. 2009. Human health risks of engineered nanomaterials. In: *Nanomaterials: Risks and Benefits*. Springer Netherlands 3–29.

Garcia GJM, Kimbell JS. 2009. Deposition of inhaled nanoparticles in the rat nasal passages: Dose to the olfactory region. *Inhal Toxicol* 21(14):1165-1175.

Gavanji S, Larki B, Mehrasa M. 2013. A Review of destructive effect of nano silver on human health, environment and animals. *International Journal of Scientific Research in Environmental Sciences (IJSRES)* 1(9):231-239.

Genter MB, Newman NC, Shertzer HG, Ali SF, Bolon B. 2012. Distribution and systemic effects of intranasally administered 25 nm silver nanoparticles in adult mice. *Toxicol Pathol* 40:1004-1013.

Glover RD, Miller JM, Hutchison JE. 2011. Generation of metal nanoparticles from silver and copper objects: Nanoparticle dynamics on surfaces and potential sources of nanoparticles in the environment. *ACS Nano* 5(11):8950-8957.

Hopkins LE, Patchin ES, Chiu PL, Brandenberger C, Smiley-Jewell S, Pinkerton KE. 2014. Nose-to-brain transport of aerosolised quantum dots following acute exposure. *Nanotoxicology* 8(8):885-893.

ICRP. 1994. Human respiratory tract model for radiological protection. *Ann ICRP* 24(1–3).

Illum L. 2000. Transport of drugs from the nasal cavity to the central nervous system. *Eur J Pharm Sci* 11:1-18.

Ji JH, Jung JH, Kim SS, Yoon JU, Park JD, Choi BS, et al. 2007. Twenty-eight-day inhalation toxicity study of silver nanoparticles in sprague-dawley rats. *Inhal Toxicol* 19:857-871.

Kovacs T. 2004. Mechanisms of olfactory dysfunction in aging and neurodegenerative disorders. *Ageing Res Rev* 3:215-232.

Liu J, Wang Z, Liu FD, Kane AB, Hurt RH. 2012. Chemical transformations of nanosilver in biological environments. *Acs nano* 6(11):9887-9899.

Loza K, Diendorf J, Sengstock C, Ruiz-Gonzalez L, Gonzalez-Calbet JM, Vallet-Reji M, et al. 2014. The dissolution and biological effects of silver nanoparticles in biological media. *J Mater Chem B Mater Biol Med* 2:1634-1643.

Mistry A, Glud SZ, Kjems J, Randel J, Howard KA, Stolnik S, et al. 2009a .Effect of physicochemical properties on intranasal nanoparticle transit into murine olfactory epithelium. *J Drug Target* 17(7):543-552.

Mistry A, Stolnik S, Illum L. 2009b. Nanoparticles for direct nose-to-brain delivery of drugs. *Int J Pharm* 379:146-157.

NIH (National Institutes of Health). 2015. Nano Environmental Health and Safety. Available: <http://www.niehs.nih.gov/research/supported/exposure/nanohealth/index.cfm> [accessed 14 March 2016].

Oberdorster G, Sharp Z, Atudorei V, Elder A, Gelein R, Kreyling W, et al. 2004. Translocation of inhaled ultrafine particles to the brain. *Inhal Toxicol* 16:437-445.

Patel S, Chavhan S, Soni H, Babbar AK, Mathur R, Mishra AK, et al. 2011. Brain targeting of risperidone loaded solid lipid nanoparticles by intranasal route. *J Drug Target* 19(6):468–474.

Rasband WS. 1997-2014. ImageJ. US National Institutes of Health. Bethesda, Maryland, USA. Available: <http://imagej.nih.gov/ij/> [accessed 30 March 2016].

Shepherd GM. 1994. *Neurobiology*. New York: Oxford University Press.

Silva R, Anderson D, Franzl L, Peake J, Edwards P, Van Winkle L, Pinkerton K. 2014. Pulmonary effects of AgNP size, coating and dose over time upon intratracheal instillation. *Toxicol Sci* 144(1):151-162.

Silver Lungs. 2009. Silver Lungs^{PH} System Homepage. Available: <http://silverlungs.com/> [accessed 30 March 2016].

Simko M, Mattsson MO. 2014. Interactions between nanosized materials and the brain. *Curr Med Chem* 21:4200-4214.

Soderstjerna E, Bauer P, Cedervall T, Abdshill H, Johansson F, Johansson UE. 2014. Silver and gold nanoparticles exposure to in vitro cultured retina – studies on nanoparticle internalization, apoptosis, oxidative stress, glial- and microglial activity. *PLoS ONE* 9(8):1-16.

Sung JH, Ji JH, Park JD, Yoon JU, Kim DS, Jeon KS, et al. 2009. Subchronic inhalation toxicity of silver nanoparticles. *Toxicol Sci* 108(2):451-461.

The Project on Emerging Nanotechnologies. 2015. The Project on Emerging Nanotechnologies Homepage. Available: <http://www.nanotechproject.org> [accessed 30 March 2016].

The Silver Edge. 2012. The Silver Edge Homepage. Available: <http://thesilveredge.com/nebulize-colloidal-silver.shtml#.VNMSYSvF-n9> [accessed 30 March 2016].

Thornton DJ, Rousseau K, McGuckin MA. 2008. Structure and function of the polymeric mucins in airways mucus. *Annu Rev Physiol* 70:459-486.

Tolaymat TM, Badaway AMR, Genaidy A, Scheckel KG. 2010. An evidence-based environmental perspective of manufactured silver nanoparticle in syntheses and applications: A systematic review and critical appraisal of peer-reviewed scientific papers. *Sci Total Environ* 408:999-1006.

Wang X, Ji Z, Chang CH, Zhang H, Wang M, Liao YP, et al. 2014. Use of coated silver nanoparticles to understand the relationship of particle dissolution and bioavailability to cell and lung toxicological potential. *Small* 10(2):385-398.

Wei L, Lu J, Xu H, Patel A, Chen ZS, Chen G. 2015. Silver nanoparticles: synthesis, properties, and therapeutic applications. *Drug Discov Today* 20(5):595-601.

Xiu ZM, Zhang QB, Puppala HL, Colvin VL, Alvarez PJJ. 2012. Negligible particle specific antibacterial activity of silver nanoparticles. *Nano Lett* 12(8):4271-4275.

Zhang W, Yao Y, Sullivan N, Chen Y. 2011. Modeling the primary size effects of citrate-coated silver nanoparticles on their ion release kinetics. *Environ Sci Technol* 45:4422-4428.

TABLES

Table 1. Characterization of 20 and 110 nm AgNP in suspension and following aerosolization (adapted from Anderson et al. 2015)			
Parameter	Method	C20	C110
Hydrodynamic diameter before exposure (nm) ^a	Dynamic Light Scattering (DLS)	27.06 ± 0.15	111.2 ± 0.2
Hydrodynamic diameter after exposure (nm) ^a	Dynamic Light Scattering	27.24 ± 0.21	106.6 ± 0.2
Geometric Mean Size (nm, standard deviation)	SMPS	77.4 (1.8)	78.2 (1.8)
Total particle mass concentration (mg/m ³)	Gravimetric Analysis	13.9 ± 2.3	12.4 ± 2.5
Airborne silver ion concentration (mg/m ³)	XRF	7.2 ± 0.8	5.3 ± 1.0
Airborne particle number based on airborne concentration of silver (#/m ³) ^b	Calculated	1.63x10 ¹⁴	7.24x10 ¹¹

^aHydrodynamic diameter of particles was measured from sealed containers before exposure and from particles recovered from the nebulizer at the end of exposure. DLS was measured with a Zetasizer Nanosizer ZEN 1690. ^bAirborne particle number = Airborne concentration from XRF (mg/m³)/(mass of C20 or C110 (g)*1000)

FIGURE LEGENDS

Figure 1. Microglial morphology of rat olfactory bulb stained with anti-Iba1 antibody. Left, resting/ramified (R) microglia exhibiting thin protrusions extending highly branched protrusions from the cell body; right, activated microglia (A) exhibiting amoeboid morphology with shorter, stouter processes. Left, C110 treated rat at T21; right, C20 treated rat at T21. Bar = 20 μm .

Figure 2. Comparison of silver concentration in the nose (A) and olfactory bulb (B) between citrate (control), 20 nm, and 110 nm AgNP at different post-exposure days.

*Significantly different from citrate control ($p < 0.05$), #Significantly different from the mean value at T0 in animals that had the same exposure ($p < 0.05$). Values are mean \pm SE. The level of detection is 0.011 $\mu\text{g Ag/g tissue}$. Mean value obtained from 5 animals per particle type and time point.

Figure 3. Comparison of percent difference from control of activated microglial in the olfactory bulb between 20 nm and 110 nm AgNP at different post-exposure days.

*Significantly different from citrate control ($p < 0.05$), #Significantly different from the mean value at T56 in animals that had the same exposure ($p < 0.05$). Values are mean \pm SE. Mean value obtained from 3 animals per particle type and time point except group C110 at T56 where the mean value from 2 animals was obtained.

Figure 4. Comparison of microglial number/10 fields in the olfactory bulb between control and rats exposed to AgNP following different post exposure days. Values are mean \pm SE.

Mean value obtained from 3 animals per particle type and time point except group C110 at T56 where the mean value from 2 animals was obtained.

Figure 1.

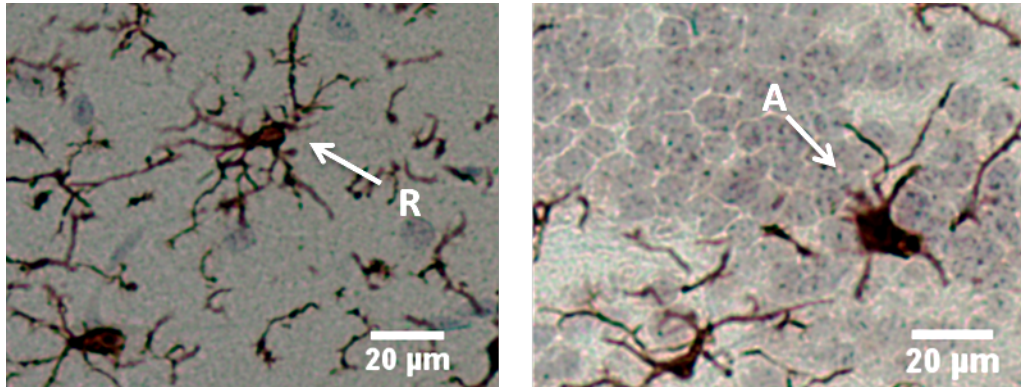


Figure 2.

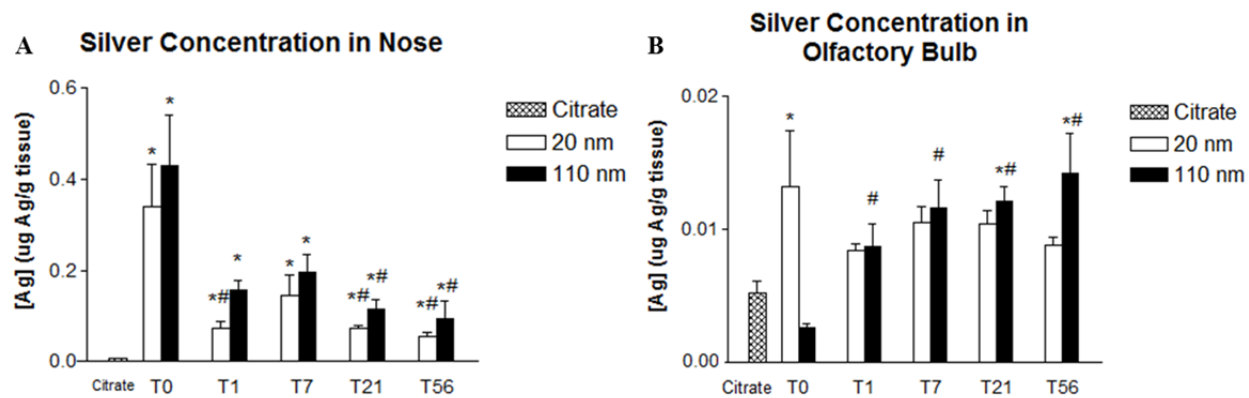


Figure 3.

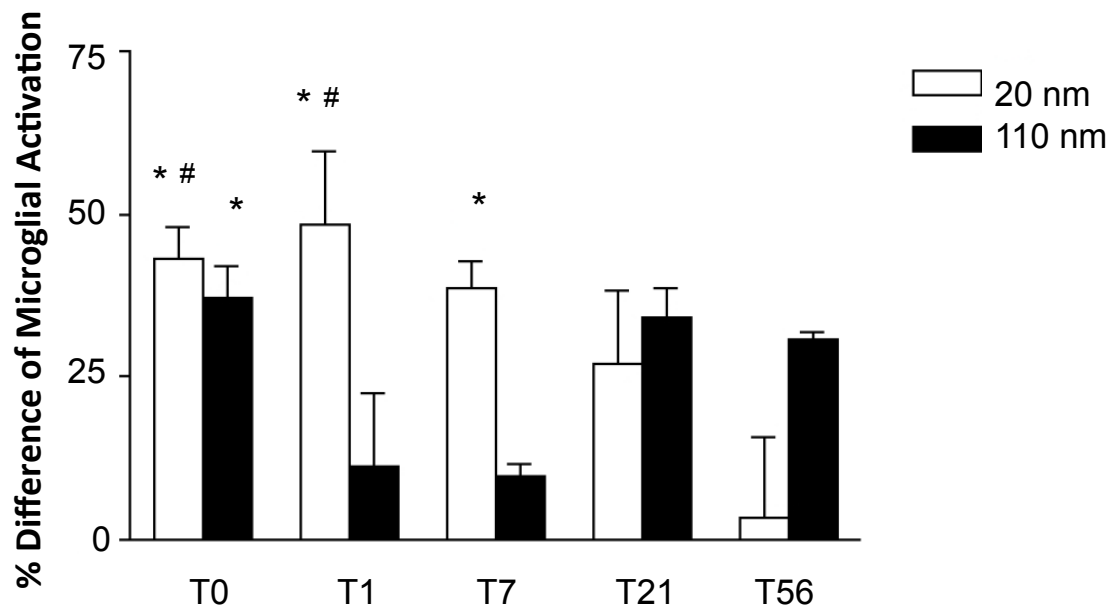


Figure 4.

